Volume 242, number 2, 218-224 FEB 06625 January 1989

Improved strategies for the determination of protein structures from NMR data: the solution structure of acyl carrier protein

T.A. Holak, M. Nilges and H. Oschkinat

Max-Planck-Institut für Biochemie, D-8033 Martinsried bei München, FRG

Received 18 October 1988

The hybrid method that combines the early stages of a distance geometry program with simulated annealing in the presence of NMR constraints was optimized to obtain structures fully consistent with the observed NMR data. This was achieved by using more restrictive bounds of the NOE constraints than those usually used in the literature and by grouping the NOEs into classes dependent on the quality of the experimental NOE data. The 'floating' stereospecific assignment introduced at the simulated annealing stage of the calculations further improved the definition of the local conformation. An improved sampling and convergence property of the hybrid method was obtained by means of fitting the substructure obtained from the distance geometry program to different conformations. Compared to the standard hybrid methods, this procedure gave superior structures for a 77 amino acid protein, acyl carrier protein from *Escherichia coli*.

NMR; Protein structure; Molecular dynamics; Distance geometry

1. INTRODUCTION

The methods based on molecular mechanics [1–4], molecular dynamics [2,5–10] and least-squares minimization of torsion angle space [1,11–13] have been used successfully in the determination of three-dimensional structures of proteins by NMR. We have recently shown that a substantial saving in computing time may be achieved with a hybrid approach that combines early stages of a distance geometry program with energy minimization [4]. The substructures obtained from phase 2 of the distance geometry method (DISGEO) [14,15], which contain only about a third of the atoms and have approximately the correct polypeptide fold, were used as starting structures for a two-stage energy minimization. Further exploration of conformational space was pursued using a similar hybrid method with the exception that the energy minimization was replaced by simulated annealing (SA) calculations [16]. The solution structure of acyl carrier protein (ACP) from *Escherichia coli* was determined using these two approaches. Compared to the SA hybrid method, the structures produced by the two stage minimization hybrid method were better defined in terms of local structural elements and correspondence to the observed set of NOE constraints. None of the structures, however, could fully reproduce secondary structure elements expected from the analysis of 2D NMR [17]. In principle, the hybrid method of distance geometry and simulated annealing should be better suited to locating the global minimum of the potential energy of the protein. In this paper therefore this hybrid method is further developed. A more sophisticated treatment of the NOE input data is achieved by classifying the distance constraints into groups with different NOE force constants depending on the quality of the experimental NOE data and by use of more restrictive bounds of NOE constraints than those usually employed in the literature. Further, the 'floating' chirality assignment is introduced in the SA stage of the calcula-

Correspondence address: T.A. Holak, Max-Planck-Institut für Biochemie, D-8033 Martinsried bei München, FRG

Published by Elsevier Science Publishers B.V. (Biomedical Division)
00145793/89/$3.50

tions to deal with the problem of stereospecific assignments at prochiral centers. This procedure allows β-protons of methylene groups and methyls of valines and leucines to flip at the prochiral centers so as to fit the NOE data. The increased sampling property of the hybrid method is obtained by starting calculations from a more expanded set of starting structures. In addition, the calculations are based on 666 NOEs (compared to 450 NOEs used previously), which corresponds to an almost complete assignment of the NOESY spectrum of the ACP. The current structures of ACP have general folding and helix topography fully consistent with the observed NOESY spectrum.

2. METHODOLOGY

2.1. *Determination of distances from 2D NOE spectra*

The intensities of the NOE cross peaks were determined from volume integrals [18]. Previously, all distances were calibrated using a single proportionality constant [4]. Using this calibration, the distance constraints for weaker NOEs between NH($i+1$) – CαH(i), NH($i+3$) – CαH(i), and NH($i+4$) – CαH(i) in α-helices were systematically underestimated by ~0.3–0.5 Å compared to the respective distances in a perfect α-helix [19]. To offset these deviations, the distances were now classified into three groups. For the intensity of an NOE peak of 20–160 (in arbitrary units) the distance constraints were calculated using the single proportionality constant as before with the estimated bounds to the distance constraints d −0.3 Å/+0.3 Å. For 15–19 units the distance constraint was set to 3.4 Å, d −0.4 Å/+0.3 Å, and for 4–15 units to 4.2 Å, d −0.6 Å/+0.8 Å. Note that the lower bounds are used explicitly. In our experience, this is essential so that the calculated structures are consistent with the intensities of the cross peaks observed in the NOESY spectrum. We have carried out a few SA calculations with the same set of NOE constraints with the exception that the lower limit for all the constraints was set to the uniform value of 1.8 Å. The structures calculated were completely consistent with the distance constraints used in the input but these structures were not consistent with the measured NMR data. For example, a few NH-NH distances were calculated to be 1.44 Å, the violations being less than 0.5 Å from the lower limit of 1.8 Å, but in stark disagreement with the NOESY data.

2.2. *Input for the DISGEO and SA calculations*

Refinement of the ACP structures with simulated annealing involved calculations with two sets of input distance constraints (set S and set N). In set S the 'floating' stereo-specific assignment was used for β-methylene protons and for the methyls on valines and leucines, whereas for set N a slightly modified pseudoatom approach was employed.

Although all protons were explicitly defined in the SA calculations, additional terms were added to the upper bounds. For any experimental distance constraints involving methyl groups, aromatic protons, and methylene protons for which only one signal is observed, an appropriate correction was added to the upper distance bounds and the distance is referred to the average positions of these protons [20]. These corrections were used in both sets S and N of the input constraints data. When the difference in chemical shifts between the 2 methylene protons or 2 methyl groups on valine or leucine was large enough that NOEs involving each group could be resolved, they were assigned arbitrarily to Hβ_1 and Hβ_2, or Me$_1$ and Me$_2$. For set S then, specific distance constraints to the Hβ_1 and Hβ_2 proton or Me$_1$ and Me$_2$ group were used in the calculations. In the case when only an NOE to one of the partners from the resolved pair was observed, the distance constraint to the other partner was set to 4.5 Å, with the lower bound −0.6 Å, and the upper bound +1.8 Å and 3.0 Å for methylene protons and methyls, respectively. The upper terms are simply the maximum distances between the protons in the methylene group and between the centers of the two methyls in the isopropyl group, respectively [21]. In the non-stereospecific calculations (set N), the designation Hβ_1, Hβ_2, Me$_1$, and Me$_2$ was also retained. However, the same lower bound was used for the two protons or the two methyls in the pair. This was set to the lowest of the two possible bounds. Similarly for the upper bounds, the bound which had the highest value was used for both distances to the two partners in the pair.

The input distance constraints for DISGEO consisted of two tables. The principal table contained the upper bounds only. A second table with the upper and lower limits was used for the non-observed NOEs (see below). The pseudoatom representation of Wüthrich et al. [20] was used. Appropriate corrections were added to the upper bounds with the exception that no pseudoatom correction of 1 Å was used for β-methylene and methyls on valine and leucine with two separate signals. Instead the highest possible upper bound to Hβ or Me (see above) was used as a distance to the pseudoatom center. This restriction on the upper bound follows from a simple geometrical consideration that the distance from a proton to the pseudoatom center cannot be longer than the maximum distance between this proton and a proton of a methylene group or the protons of the methyl on valines or leucines.

The absence of NOEs between assigned protons also contains useful information as it means that the distance between the protons is larger than ~4–5 Å. We have estimated that the cutoff distance in our spectra is 4.5 Å. Two classes of non-NOE information were used. In the first class all unobservable NH($i+1$) – NH(i) and NH($i+1$) – CαH(i) constraints were set to the maximum allowed value for these distances, 4.6 Å, d −0.7 Å/+0.4 Å, and 3.7 Å, d −0.4 Å/+0.4 Å, respectively. In the second class of non-NOE distance constraints, they were set to 4.2 Å with the lower bound d −0.4 Å and upper bound +50 Å. These constraints were introduced after a few initial calculations. The structures were then checked for short distances between protons that contradict the lack of an observable NOE. 18 such distances were added to the input NOE data and used in the DISGEO and SA input distance constraint tables. Both tables were supplemented by 46 constraints for the 23 intrahelical NH($i+4$) – O(i) hydrogen bonds identified on the basis of slowly exchanging amide protons. For each hydrogen bond the N-O and NH-O distances were constrained to 1.9 Å, d −0.6 Å/+0.4 Å, and 2.8 Å, d −0.6 Å/+0.4 Å, respectively. Well defined α-helical segments were further constrained by restricting the ϕ and ψ backbone torsion angles to

the allowed region of the ψ,ϕ map: ϕ $-60.0° \pm 30.0°$, and ψ $-35.0° \pm 20.0°$ [22]. 78 such constraints were present in the DISGEO and SA calculations. A constraint on the torsion angle in the fragment Ile-54–Pro-55 was also added with ψ between 60° and 180° [23].

2.3. *Structure calculations*

The basic protocol used for the calculations has been presented [16]. Briefly, it consists of 5 stages. In stage 1, the substructure coordinates are obtained from the distance geometry program DISGEO [24]. In the second stage all of the atoms are added to a subset of atoms already present in substructures. Steps three and four consist of simulated annealing. The fifth stage involves 200 cycles of constrained Powell minimization. These last four stages are carried out with the program XPLOR ([9] and Brünger, A.T., unpublished).

Simulated annealing involves raising the temperature of the system (step 3) followed by slow cooling (step 4) in order to overcome local minima and locate the region of the global minimum of the target function [7]. The total target function F_{tot} comprises the following terms:

$$F_{tot} = F_{covalent} + F_{repel} + F_{NOE} + F_{\psi,\phi}$$

$F_{covalent}$ is the target function for maintaining correct bond lengths, angles, planes and chirality, and is given by:

$$F_{covalent} = \Sigma_{bonds} k_b(r - r_o)^2 + \Sigma_{angles} k_\vartheta(\theta - \theta_o)^2 + \Sigma_{impropers} k_\vartheta(\vartheta - \vartheta_o)^2 + \Sigma_\omega k_\omega(1 + \cos\omega)$$

The force constants of the energy terms for bonds, angles, impropers and dihedral angle ω at the peptide bond were set to the uniform value of 500 kcal/mol during the simulated annealing stage. The dihedral angle ω term is added in the present calculations.

The non-bonded interactions, F_{repel} are represented by a simple van der Waals repulsion term with variable force constant, k_{repel}. The initial value of k_{repel} is very low (0.001 kcal·mol^{-1}·Å^{-2}), and is increased slowly to its final value of 4 kcal·mol^{-1}·Å^{-2} [16]. The NOE distance constraints, F_{NOE}, are represented by a square-well potential with a variable force constant k_{NOE} [8]. Initially k_{NOE} was set to 1 in the present calculations. In addition, $F_{\psi,\phi}$ is added to the total target function in the present calculations. $F_{\psi,\phi}$ is a square-well dihedral potential term with force constant of 40 kcal·mol^{-1}·Å^{-2}. Step 1 of SA was carried out with 50 cycles of 75 fs dynamics at 1000 K. Step 2 consisted of 1.5 ps dynamics at 300 K. In stage 5 the structures are improved by ~200 cycles of energy minimization.

In stage 2 of the protocol, the amino acids in extended conformation (structures E) and α-helical conformation (structures A) were best fitted to the substructures residue by residue. 200 cycles of unconstrained energy minimization with a very low force constant on the van der Waals repulsion term were then carried out to remove any close constants between atoms. These E and A structures were used as starting structures for simulated annealing. The SA calculations were carried out in two variants: (a) variant S with 'floating' chirality assignment, and (b) variant N with the usual pseudoatom approach. For each substructure therefore four sets of structures were calculated and these are designated as AS, AN, ES, EN.

Both sets of the input distance constraints (set S and set N) were classified into 4 groups with different force constants k_{NOE} depending on the quality of the NOE data. In the first group of constraints most of the backbone and long range constraints were included. The force constant k_{NOE} was allowed to rise fastest, compared to those of the other groups, to its maximum value of 50 kcal·mol^{-1}·Å^{-2}. In the second group all the sidechain constraints were included. The final k_{NOE} was set to 40 kcal·mol^{-1}·Å^{-2} in this group. The third group contained all the constraints for which the measured intensities were less accurate due to the partial overlap of the cross peaks and because of other spectroscopic uncertainties. For these constraints, the k_{NOE} was set to 30 kcal·mol^{-1}·Å^{-2}. Finally, in the fourth group all the unobservable distance constraints were collected together with those distance constraints for which the uncertainty in the assignment or in the estimated intensities was the greatest. The k_{NOE} was 15 kcal·mol^{-1}·Å^{-2} in this group. This type of grouping of the NOEs proved to be quite important as it allowed a large number of 'ambiguous' NOEs to be included in the fourth group for the initial calculations, with the calculated structures dominated by the distance constraints from the first three groups. After a few initial calculations, a number of distance constraints in group 4 which were repeatedly not satisfied by the calculated distances were rechecked and either kept or removed from the distance constraints table.

Several protocols were tested for the 'floating' chirality calculations (sets AS and ES). The most effective protocol involved lowering the force field constants during the two SA stages for angles HA-CT-HA, CT-CT-CT, and HA-CT-CT, where HA is a proton and CT is a tetrahedral carbon with four explicit substituents, to 5.0, 5.0, and 30.0 kcal·mol^{-1}·rad^{-2}, respectively. Also, the 1–4 nonbonded interaction for the protons and the carbon of the methyl groups of valines and leucines was selectively switched off. This procedure is sufficient to allow β protons of methylene groups and methyls of valines and leucines to flip at the prochiral center. For the final fifth stage of the energy minimization all angle terms were set to 200 kcal·mol^{-1}·Å^{-2} and the 1–4 non-bonded interaction was reintroduced. The bond force constant was kept at 500 kcal·mol^{-1}·Å^{-2}. These maintain near perfect covalent geometry of the structures and ensure that no close contacts occur.

3. RESULTS AND DISCUSSION

The results of the calculations are summarized in tables 1–3. The global folding of the current structures is similar to that of the previously calculated structures (fig.1). The secondary conformation of the present structures is fully consistent with the prediction derived from the NOESY spectra. The structures are dominated by four α-helices: residues 3–15, residues 37–50, residues 56–62, and residues 65–75. These are quite regular helices as there is no violation of the ψ and ϕ torsion angles within the bounds specified in the dihedral constraint input. The region from residues 16–36 is less well defined (table 3 and fig.1). The quality of the structures as regards deviations from ideal

Table 1

Average deviations from ideality and energies of the structures

Structure	Deviations from ideality				
	Bonds (Å)	Angles (°)	Impropers (°)	F_{NOE} (kcal/mol)	E_{L-J} (kcal/mol)
⟨AS⟩	0.011 ± 0.001	2.03 ± 0.04	0.291 ± 0.040	66 ± 20	−322 ± 20
⟨ES⟩	0.011 ± 0.001	2.04 ± 0.04	0.312 ± 0.045	67 ± 20	−335 ± 35
⟨AN⟩	0.010 ± 0.001	1.99 ± 0.04	0.282 ± 0.040	70 ± 25	−318 ± 20
⟨EN⟩	0.010 ± 0.001	2.00 ± 0.04	0.273 ± 0.045	70 ± 15	−313 ± 30

The notations of the structures are as follows: ⟨AS⟩, ⟨ES⟩, ⟨AN⟩, and ⟨EN⟩ comprise of all the structures in the given group of the structures. The force constants used to calculate F_{NOE} are 50 kcal·mol^{-1}·Å^{-2}. The Lennard-Jones Van der Waals energy E_{L-J} is calculated using the CHARMM empirical energy function [25]

Table 2

RMS differences between experimental and calculated distance constraints

Structure	No. of structures	NOE input	Average no. of distance violations >0.4 Å[b]	RMS differences between calculated and experimental distance constraints[a]			
				All (666)	Backbone (289) $\|i-j\| \leqslant 5$	Sidechain (303) $\|i-j\| \leqslant 5$	Long (74) $\|i-j\| > 5$
⟨AS⟩	14	S	0.5	0.06	0.05	0.07	0.05
⟨ES⟩	10	S	0.5	0.06	0.05	0.07	0.05
⟨AN⟩	13	N	1.0	0.06	0.05	0.07	0.04
⟨EN⟩	7	N	1.1	0.06	0.05	0.07	0.04
⟨AN⟩ and ⟨EN⟩	20	S	18.2	0.17	0.05	0.18	0.33
⟨AS⟩ and ⟨ES⟩	24	N	0.2	0.05	0.05	0.06	0.05

[a] The RMS deviations (in Å) from the interproton distance constraints are calculated with respect to the upper and lower limits of the distance constraints [16]. Number of distance constraints is given in parentheses. The error limits for RMS are ± 0.005 Å except for RMS ~ 0.17 ± 0.07 Å and 0.33 ± 0.12 Å

[b] There are no violations of distance constraints ⩾0.5 Å

stereochemistry, van der Waals contacts, and NOE RMS differences is also noticeably better than those previously published using the SA hybrid method. In particular, in terms of nonbonded interactions the current structures have much lower Lennard-Jones energies. Both sets S and N display comparable results for the backbone atoms (table 2). The sidechain and long range distances, however, are better defined in the S structures. When the N structures are checked for distance constraint violations against the NOE input data S the RMS difference is 0.17 Å (table 2). Table 3 shows the spread of the structures within the allowed conformational space. It can be seen from table 3 that the spread of the structures which originated from the same substructure by fitting to a different conformation of the polypeptide chain is equivalent to those between the starting substructures. In the poorly defined region, residues 16–36, these differences are also preserved. The fitting procedure therefore contributes also to the sampling properties of the hybrid method. In conclusion, fitting the starting structures to different conformations, which is substantially faster than producing a new substructure, gives similar results to those obtained when different starting substructures are used. This was rather surprising as the RMS differences between starting A and E structures derived from the same substructure are smaller than those between the starting structures derived from different substructures (table 3). The A starting structures and the S 'floating' chirality

Table 3

Atomic RMS differences between all pairs of individual structures

	Atomic RMS differences (Å)			
	Residues 2–75		Residues 16–36	
	Backbone atoms	All atoms	Backbone atoms	All atoms
⟨AS,ES⟩ vs ⟨AS,ES⟩	1.4 ± 0.2	2.2 ± 0.4	2.1 ± 0.4	3.1 ± 0.5
⟨⟨AS⟩⟩ vs ⟨⟨ES⟩⟩	1.4 ± 0.3	2.2 ± 0.3	2.0 ± 0.4	3.0 ± 0.5
⟨AN,EN⟩ vs ⟨AN,EN⟩	1.7 ± 0.3	2.5 ± 0.4	2.3 ± 0.4	3.5 ± 0.5
⟨⟨AN⟩⟩ vs ⟨⟨EN⟩⟩	1.5 ± 0.4	2.4 ± 0.4	2.2 ± 0.4	3.4 ± 0.4
⟨AS,ES⟩ vs ⟨AN,EN⟩	1.5 ± 0.4	2.5 ± 0.5	2.2 ± 0.4	3.4 ± 0.4
⟨⟨AS⟩⟩ vs ⟨⟨AN⟩⟩	1.5 ± 0.3	2.4 ± 0.4	2.1 ± 0.3	3.1 ± 0.4
⟨⟨ES⟩⟩ vs ⟨⟨EN⟩⟩	1.5 ± 0.3	2.4 ± 0.4	2.2 ± 0.3	3.2 ± 0.4
⟨ASB,ESB⟩ vs ⟨ASB,ESB⟩	1.6 ± 0.4	2.4 ± 0.4	1.9 ± 0.3	2.8 ± 0.4
⟨⟨ASB⟩⟩ vs ⟨⟨ESB⟩⟩	0.8 ± 0.4	1.4 ± 0.5	1.0 ± 0.4	1.3 ± 0.4

The notations of the structures are the same as those in table 1; ⟨AS,ES⟩ vs ⟨AS,ES⟩ etc. corresponds to any 3 possible combinations of the structures shown in parentheses, i.e. ⟨AS⟩ vs ⟨AS⟩, ⟨AS⟩ vs ⟨ES⟩, ⟨ES⟩ vs ⟨ES⟩. ⟨⟨AS⟩⟩ vs ⟨⟨AN⟩⟩ etc. comprise only those pairs of the structures which originated from the same substructure. ⟨ASB⟩ and ⟨ESB⟩ are the starting structures after the second stage of the calculations

Fig.1. Stereoview of the backbone (N, Cα, C) atoms of the final S structures superimposed on the constrained minimized average structure SA_r.

calculations have better convergence properties than those of the E structures or the N calculations (table 2). We have refined as many substructures as was necessary to obtain 10 final ES structures. The increased convergence property of the calculations starting from the A starting structures may be peculiar to ACP which contains a high percentage (70%) of α-helical secondary elements.

The procedure of 'floating' chirality assignment was originally proposed for the distance geometry

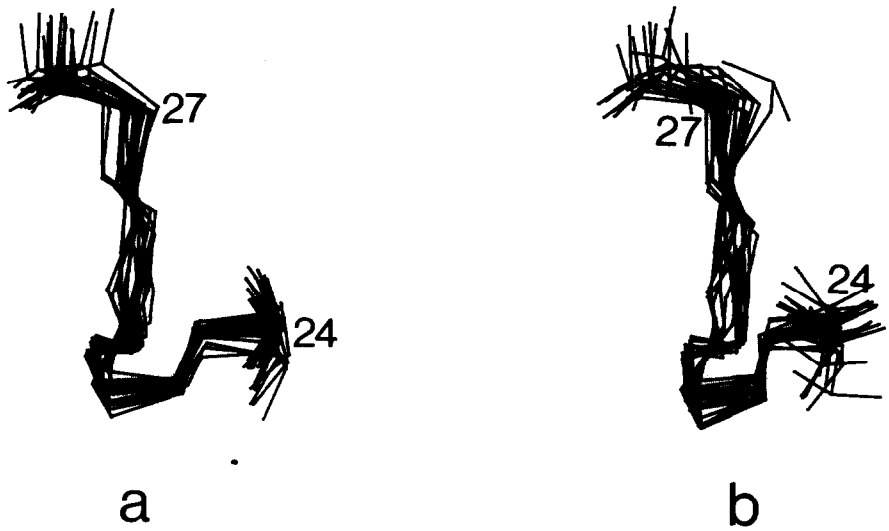

Fig.2. A view of the fragment of residues 24–27 obtained by best fit superpositions of the backbone atoms of residues 23–28. The β-protons and β-carbons for residues 24 and 27 and the backbone atoms are shown. (a) S structures, (b) N structures.

calculations by Pardi et al. [21]. In their case, this was achieved by relaxing the chirality constrains on the prochiral centers. It was found in those calculations that when the 'floating' stereospecific assignment was not used, many structures had distance constraints larger than 5 Å, larger than the longest distance for which NOEs could be observed in the NMR spectra ($\leq$4.5 Å). Our calculations allow a more critical comparison between the 'stereospecific' and 'non-stereospecific' types of the calculations. As in the 'non-stereospecific' calculations no additional terms were added to the upper bounds for β-methylene protons and the methyls on valines and leucines with two separate signals, none of the distance constraints in the set N calculations had upper bounds larger than those for which NOEs could be observed in an NMR spectrum ($d < 4.5$ Å). Still, it is evident from table 2 and fig.2 that there is an improvement on the restriction of the allowed conformations for the S set over the N set. The improvement occurs when the difference in the two sidechain NOEs is quite large (~15–20 units). One positive aspect of the S calculations is that when there are several NOEs connected to a single proton (say $H\beta_1$ vs $H\beta_2$), it is easier to check whether the pattern of the distance constraints to this proton is preserved in the calculated structures. Any inconsistency in the pattern may indicate regions of increased flexibility of the protein. In conclusion, the 'floating' chirality assignment calculations yield better results than the all-pseudoatom approach. Since the method does not require any additional computing time or input data it should find a widespread use in the calculations of 3D structures using NMR data.

Acknowledgements: We thank Dr J.H. Prestegard for useful discussions. This work was supported by the Max-Planck Gesellschaft.

REFERENCES

[1] Wüthrich, K. (1986) NMR Proteins and Nucleic Acids, Wiley, New York.
[2] Kaptein, R., Zuiderweg, E.R.P., Scheek, R.M., Boelens, R. and Van Gunsteren, W.F. (1985) J. Mol. Biol. 182, 179–182.
[3] Holak, T.A., Prestegard, J.H. and Forman, J.D. (1987) Biochemistry 26, 4652–4660.
[4] Holak, T.A., Kearsley, S.K., Kim, Y. and Prestegard, J.H. (1988) Biochemistry 27, 6135–6142.
[5] Clore, G.M. and Gronenborn, A.M. (1987) Protein Eng. 1, 275–288.
[6] Kaptein, R., Boelens, R., Scheek, R.M. and Van Gunsteren, W.F. (1988) Biochemistry 27, 5389–5395.
[7] Nilges, M., Gronenborn, A.M., Brünger, A.T. and Clore, G.M. (1988) Protein Eng. 2, 27–38.
[8] Clore, G.M., Nilges, M., Sukumaran, D.K., Brünger, A.T., Karplus, M. and Gronenborn, A.M. (1986) EMBO J. 5, 2729–2735.

[9] Brünger, A.T., Clore, G.M., Gronenborn, A.M. and Karplus, M. (1986) Proc. Natl. Acad. Sci. USA 83, 3801–3805.
[10] Tappin, M.J., Pastore, A., Norton, R.S., Freer, J.H. and Campbell, I.D. (1988) Biochemistry 27, 1643–1647.
[11] Braun, W. and Gō, N. (1985) J. Mol. Biol. 186, 611–626.
[12] Wagner, G., Braun, W., Havel, T.F., Schaumann, T., Gō, N. and Wüthrich, K. (1987) J. Mol. Biol. 196, 611–639.
[13] Braun, W. (1987) Q. Rev. Biophys. 19, 115–157.
[14] Havel, T.F. and Wüthrich, K. (1985) J. Mol. Biol. 182, 281–294.
[15] Williamson, M.P., Havel, T.F. and Wüthrich, K. (1985) J. Mol. Biol. 182, 295–315.
[16] Holak, T.A., Nilges, M., Prestegard, J.H., Gronenborn, A.M. and Clore, G.M. (1988) Eur. J. Biochem. 175, 9–15.
[17] Holak, T.A. and Prestegard, J.H. (1986) Biochemistry 25, 5766–5774.
[18] Holak, T.A., Scarsdale, J.N. and Prestegard, J.H. (1987) J. Magn. Reson. 74, 546–549.
[19] Wüthrich, K., Billeter, M. and Braun, W. (1984) J. Mol. Biol. 180, 715–740.
[20] Wüthrich, K., Billeter, M. and Braun, W. (1983) J. Mol. Biol. 169, 949–961.
[21] Pardi, A., Hare, D.R., Selsted, M.E., Morrison, R.D., Bassolino, D.A. and Bach, A.C., ii (1988) J. Mol. Biol. 201, 625–636.
[22] Sherman, S.A., Andrianov, A.M. and Akhrem, A.A. (1987) J. Biomol. Struct. Dyn. 4, 869–884.
[23] Arseniev, A., Schultze, P., Wörgötter, E., Braun, W., Wagner, G., Vašák, M., Kägi, J.H.R. and Wüthrich, K. (1988) J. Mol. Biol. 210, 637–657.
[24] Havel, T.F. (1986) DISGEO, Quantum Chemistry Exchange, Program no.507, Indiana University.
[25] Brooks, B.R., Bruccoleri, R.E., Olafson, B.D., States, D.J., Swaminathan, S. and Karplus, M. (1983) J. Comput. Chem. 4, 187–217.